The 8th TSME International Conference on Mechanical Engineering
12-15 December 2017
Bangkok, Thailand

CST0005

Influence of saw-toothed and sine-curved trailing edge shape to asymmetric aerofoil

Pakpong Jantapremjit[1], **Pareecha Rattanasiri**[1,*],**Alongkod Tipsiri**[1], **Tana arkadumnuay**[1], **Wannachat Truekhakit**[1] **and Philip A. Wilson**[2]

[1] Department of Mechanical Engineering, Faculty of Engineering, Burapha University, Chon Buri Campus, Chon Buri, 20130, Thailand
[2] Fluid Structure Interactions Group, Faculty of Engineering and the Environment, University of Southampton, SO16 7QF, United Kingdom

* Corresponding Author: pareecha@eng.buu.ac.th, Tel. +66(0)9-2768-7904, Fax +66(0)3839-0351

Abstract. This paper aims to investigate the influence of saw-toothed and sine-curved trailing edge shape to the asymmetric aerofoil; NACA4412 and NACA4415 at a chord Reynolds number of 1.05×10^5. Firstly, the impact of the trailing edge shapes to the wake-flow behaviour is numerically investigated. Secondly, the drag coefficient is calculated and compared with the symmetric aerofoil NACA0012. The CFD RANS-SST with a commercial code ANSYS CFX simulation is performed for the fully submerged aerofoil of 150 mm chord length with three trailing edge shapes: standard straight line, saw-toothed and sine-curved shapes. The results show the thicker camber, the higher drag coefficient for saw-toothed trailing edge shape. The sine-curved trailing edge provided drag results as the standard trailing edge for NACA0012 and NACA4412. The result suggests that, in term of drag consideration, it is interchangeable for using either NACA4412 or NACA4415 at this Re, as they are provided similar drag.

1. Introduction
Wind turbine noise is mainly produced by the blades, all the noise sources is the interaction between boundary layer turbulence, which forms on the surface of the blades, with the airfoil trailing edge. It has been known as aerofoil trailing edge noise, which may be reduced by modifying the trailing edge geometry so that the aerodynamics fluctuating pressure is scattered into sound is reduced [1][2][3]. In consideration in term of the aerodynamic performance, the TBL over an airfoil may directly relate to the total drag of an aerofoil. The reduction of turbulent flow over an aerofoil, may result in the drag reduction of an airfoil.

The main purpose of this paper is to determine the aerodynamic drag of asymmetric aerofoils: NACA4412 and NACA4415 with different trailing edge shapes operated in low Reynolds Number of 1.05×10^5. Second purpose is to investigate the flow behaviours of the aerodynamic wake behind the different trailing edge shapes for asymmetric aerofoils with different thickness.

2. Theoretical approach
2.1 Total drag prediction
Physically, in the direction of resisting the moving, the aerodynamic drag can be calculated by the pressure (P) and wall shear (τ_w) which are two components of force acting on a body. In term of a dimensionless coefficient, an aerodynamic drag coefficient (C_D)is therefore calculated from the pressure drag coefficient (C_P) and the skin friction drag coefficient (C_F).

$$C_D = C_P + C_F \tag{1}$$

Alternatively, if total drag of the model aerofoil could be predicted. The drag coefficient of aerofoil could then be estimated by:-

$$C_D = (\text{Total drag})/\ (0.5\ \rho\ V^2 A) \tag{2}$$

where ρ is the fluid density, A is the aerofoil's surface area. The dimensionless air speed (V) in term of the Reynolds number (Re) based on chord length (L) could be calculated by:-

$$Re = 70000VL \tag{3}$$

To predict an accurate aerodynamic drags, a steady-state Reynolds Averaged Navier Stokes (RANS) simulation has proved to provide reasonably accurate results [4][5][6].

2.2 RANS

By assuming the flow is incompressible, the continuity equation becomes:-

$$\frac{\partial \overline{U_i}}{\partial x_i} = 0 \tag{4}$$

The momentum equation can be written as:-

$$\rho\left(\frac{\partial \overline{U_i}}{\partial t} + \frac{\partial \overline{U_i U_j}}{\partial x_j}\right) = -\frac{\partial \bar{P}}{\partial x_i} + \frac{\partial}{\partial x_j}\left\{\mu\left(\frac{\partial \overline{U_i}}{\partial x_j} + \frac{\partial \overline{U_j}}{\partial x_i}\right)\right\} - \rho\frac{\partial \overline{u_i' u_j'}}{\partial x_j} + \overline{f_i} \tag{5}$$

where i is Cartesian co-ordinates in X, Y and Z and U_i are the Cartesian mean velocity components (U_x, U_y, U_z). The Reynolds stress tensor ($\rho u_i' u_j'$) is represented in the turbulence closure and $\bar{f_i}$ is the external forces. The previous three-dimension model simulations have shown that the shear stress transport (SST) turbulence closure model is able to replicate the flow around object with a moderate computer accuracy. Therefore, a commercial code ANSYS CFX [7] was selected to perform simulation, the solver RANS-SST turbulence model was used to predict the flow in this study.

3. Numerical modelling

3.1 Aerofoil modelling

The NACA0012, NACA4412, NACA4415 (Figure 1) is modelled for the chord length (L) of 0.15 m and the span-width (S) is 0.29 m, the NACA0012 is performed to be used as the benchmark case for this study. The saw-toothed and sine-curved trailing edge shape is shown in Figure 2 and 3. The surface area (A) is shown in Table 1.

3.2 Model domain and boundary condition

The fluid domain is modelled as 0.3×0.3 m and 3.30 m long. Free slip wall conditions are used for the roof and floor. For symmetry are modelled for both left and right side-walls. The air inlet velocity (V) is 10 m/s related to the chord Reynolds Number 1.05×10^5. The zero relative pressure is for outflow condition. Aerofoil is modelled by using no slip wall condition. See Figure 4 and 5.

An appropriate mesh strategy and mesh resolution to capture the effect of the boundary layer and the wake behind the body is needed to obtain a high fidelity simulation result [5][6]. The number of element is tested for convergence of the results as detailed in Table 3. The meshing strategy and resolution is considered, samples of meshing are shown in Figure 6 and 7. The computational parameters are provided in Table 2.

Table 1. Surface area A (m^2) of NACA0012, NACA4412, NACA4415 model

Model	standard	saw-toothed	sine-curved
NACA0012	0.089422	0.083259	0.088246
NACA4412	0.089806	0.083640	0.088617
NACA4415	0.090161	0.085951	0.089433

Table 2. Computational parameters

Parameters	Setting
Mesh type	Unstructured with local refinement around aerofoil and in wake regions
$y+$	1 (for 0.15 m long, 0.016 mm first layer height with 1.5 growth rate is selected)
No. of elements	5-9 Millions with 8 prism layers in the boundary layer
Turbulence model	Shear Stress Transport
Inlet turbulent intensity	1%
Wall modelling	Automatic Wall Function
Spatial discretisation	High Resolution
Timescale control	Auto Timescale
Convergence criteria	RMS residual < 10^{-6}
Run type	Intel CORE i7 with 2GB RAM

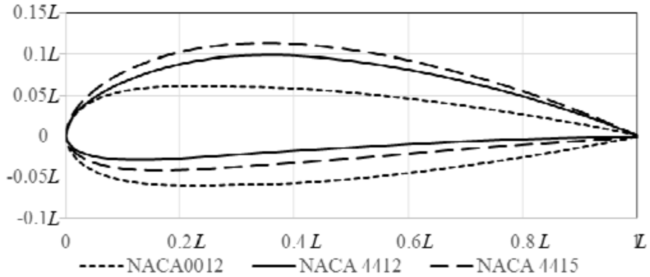

Figure 1. NACA0012, NACA4412 and NACA4415.

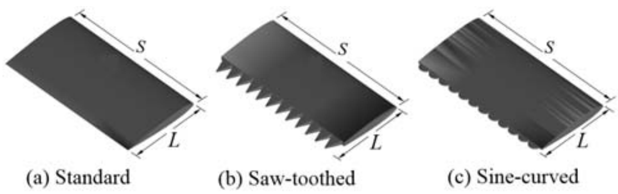

Figure 2. Aerofoil with standard, saw-toothed and sine-curved trailing edge shape.

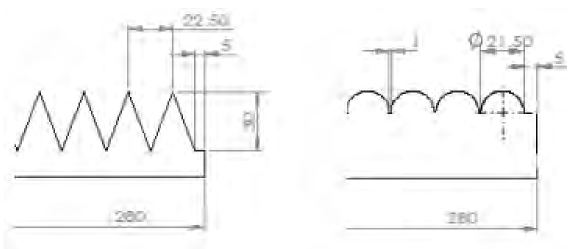

(a) saw-toothed (b) sine-curved

Figure 3. Dimension of trailing edges in mm

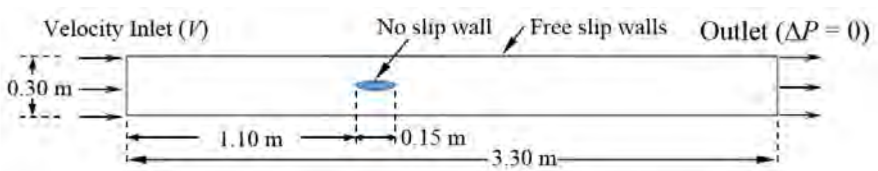

Figure 4. Fluid domain and boundary conditions

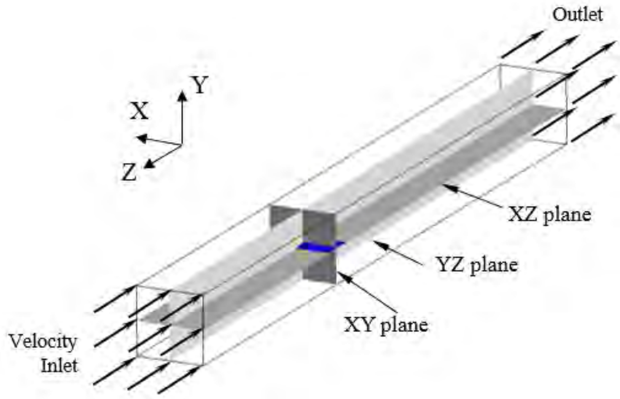

Figure 5. Isometric view of simulation domain

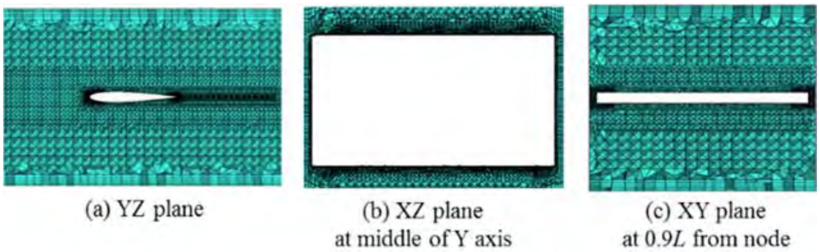

Figure 6. Sample fine mesh set for NACA0012 with standard trailing edge

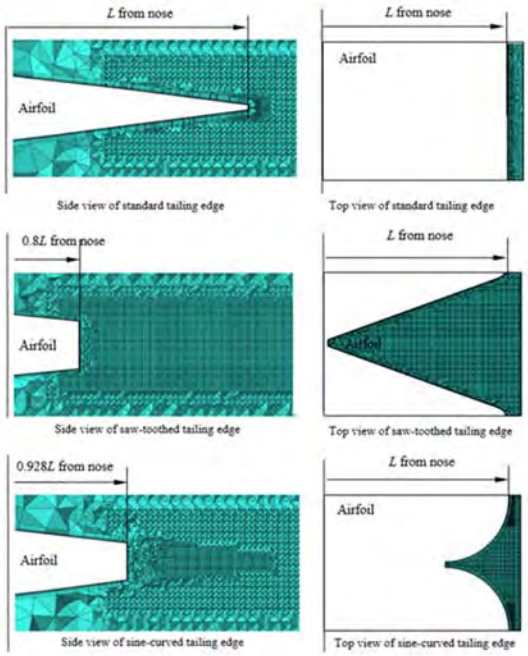

Figure 7. Fine mesh set for NACA0012 with standard trailing edge, saw-toothed trailing edge and sine-curved trailing edge

4. Result

4.1 Mesh convergences

One measure of accuracy of the numerical scheme is the effect of mesh convergence. Mesh convergences were tested for NACA0012, NACA4412 and 4415 with standard trailing edge at Re = 2.10×10^5 (Figure 8). The convergence of meshing from coarse, medium to fine mesh is 5.43, 5.63 and 7.84 million meshes, respectively. The convergence of meshing from coarse, medium to fine mesh is found for C_P, due to mesh refinement at nose and tail, the pressure gradient is predicted more accurately. From an accuracy and time consuming prospect, the fine mesh set up is selected in this study. Since the mesh convergence is found at

Re = 2.10×10^5, therefore, the same mesh set could be valid for lower Re at 1.05×10^5 to capture the flow in boundary layer.

Definition of $\%C_D$ are as following;

$$\%C_D = \frac{C_{D,i} - C_{D,i-1}}{C_{D,i}} \times 100\%, \tag{6}$$

where i is the drag coefficient of coarse, medium and fine mesh. Table 3 shows results of C_D, C_F, C_P and $\%C_D$.

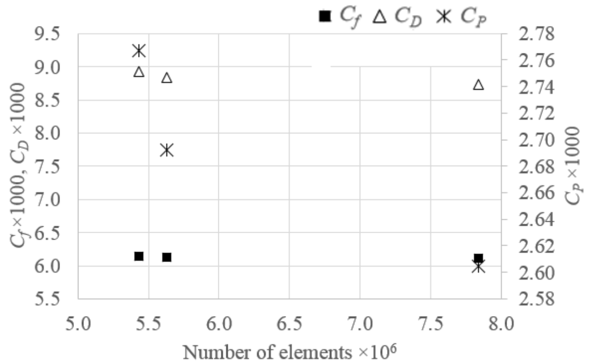

Figure 8. Mesh convergence for NACA0012 with standard trailing edge at Re=2.10×10^5

4.2 Flow around the asymmetric aerofoils

Figure 9 and 10 show the velocity contour of flow past NACA4412 and NACA4415 at Re = 1.05×10^5, respectively. Figure 11 shows the influence of TE to the velocity of the flow in the wake field. The velocity of flow past the sine-curved TE is accelerated at the TE, however, the zero velocity deficit at the 0.2L from the TE. Therefore, there is very small difference between C_F of standard and sine-curved TE. On the other hand, the velocity of flow past the saw-toothed TE is accelerated at higher velocity more than that of the flow past sine-curved TE, and zero velocity deficit at 0.6L, it results in higher C_F of the saw-toothed TE aerofoil than other type of TE.

4.3 Influence of aerofoil characteristic to drag

At the same thickness, the asymmetric aerofoil experience higher drag than the symmetric aerofoil. It is due to the velocity and pressure unbalance between upper and lower side of the aerofoil (Figure 9 and 10). In terms of magnitude, a thicker asymmetric aerofoil results in the higher the drag coefficient. The contour of flow accelerated by the camber can also be observed from Figure 9 and 10. The flow velocity of NACA4415 at both sides show higher velocity compared with NACA4412.

From Table 3, $\%C_{D,1}$ and $\%C_{D,2}$ are defined as following;

$$\%C_{D,1} = \frac{C_{D,asymmetric} - C_{D,standard}}{C_{D,standard}} \times 100\%,$$

$$\%C_{D,2} = \frac{C_{D,4415} - C_{D,4412}}{C_{D,4412}} \times 100\%, \tag{7}$$

Considering aerofoils with the same thickness; NACA4412 and NACA0012, the results of $\%C_{D,1}$ show that the additional camber results in 34%, 17% and 29% of drag increment for standard, saw-toothed and sine-curved TE shapes, respectively.

Comparing NACA4415 with NACA4412, the results of $\%C_{D,2}$ show that for the increase of camber, the drag is increased by 6%, 9% and 3% for standard, saw-toothed and sine-curved TE shapes, respectively. It might say that the sine-curved TE shape could reduce the effect of camber to the drag.

Table 3. The drag coefficient, skin friction coefficient and pressure coefficient (×1000) at Re = 1.05×10^5, impact of airfoil shape to drag

Trailing edge	NACA	C_D	$\%C_{D,1}$	$\%C_{D,2}$
Standard	0012	10.12		
	4412	13.52	34	
	4415	14.33	42	6
Saw-toothed	0012	11.49		
	4412	13.46	17	
	4415	14.67	28	9
Sine-curved	0012	10.32		
	4412	13.30	29	
	4415	13.68	33	3

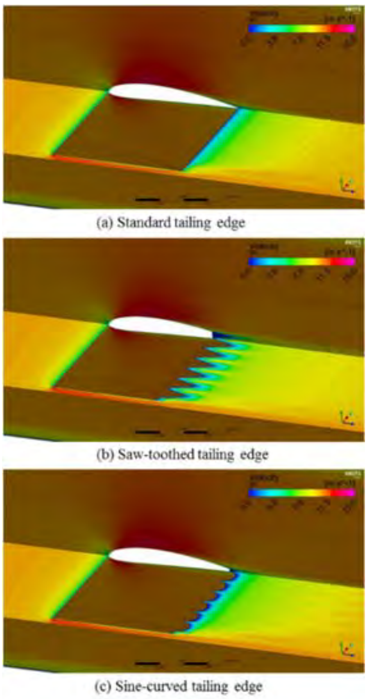

Figure 9. The velocity contour of flow past NACA4412 at Re = 1.05×10^5

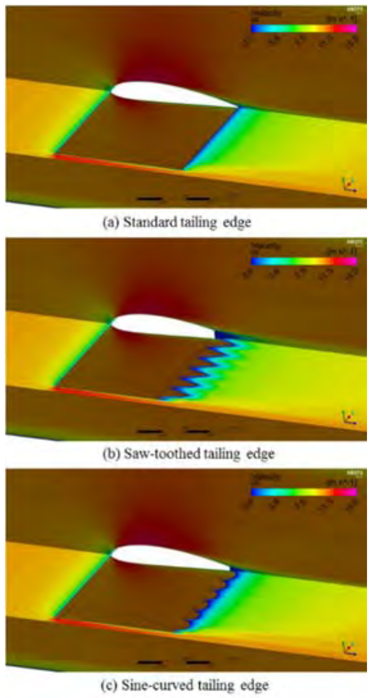

Figure 10. The velocity contour of flow past NACA4415 at Re = 1.05×10^5

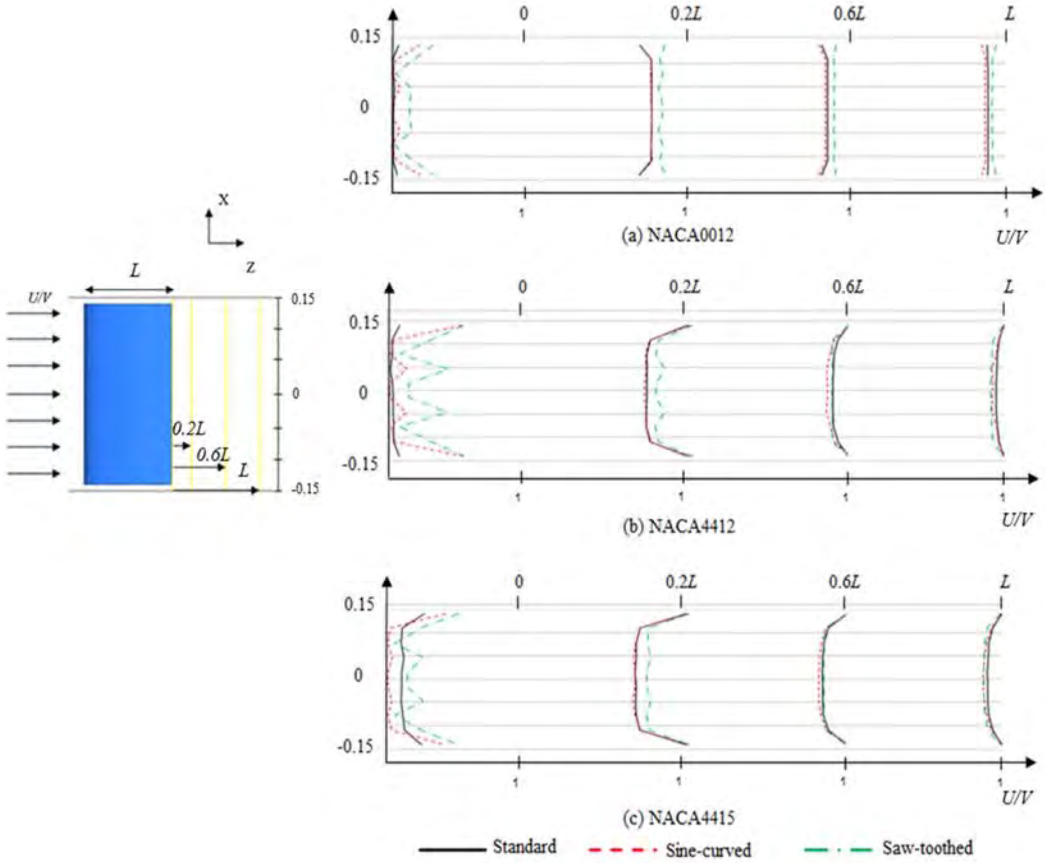

Figure 11. The velocity profile of flow past NACA0012, NACA4412 and NACA4415 at $Re = 1.05\times10^{5}$

Table 4. The impact of trailing edge shape to drag at Re = 1.05×10^{-5} for NACA0012, NACA4412 and NACA4415

NACA	Trailing edge	C_F	C_P	C_D	$\%C_D$
0012	Standard	6.99	3.11	10.12	
	Saw-toothed	7.47	4.01	11.49	13.5
	Sine-curved	7.44	2.87	10.32	2.0
4412	Standard	7.05	6.47	13.52	
	Saw-toothed	7.31	6.15	13.46	-0.5
	Sine-curved	7.45	5.85	13.30	-1.6
4415	Standard	7.11	7.21	14.33	
	Saw-toothed	7.36	7.30	14.67	2.4
	Sine-curved	7.09	6.59	13.68	-4.5

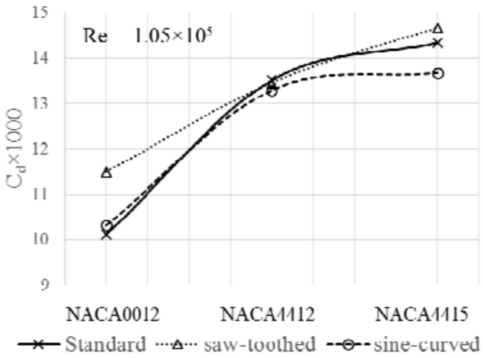

Figure 12. C_D of NACA0012, NACA4412 and NACA4415 with different trailing edges at Re=1.05×10^5

4.4 Impact of trailing edge to drag

Table 4 shows the impact of the trailing edge shape on the drag coefficient at Re = 1.05×10^{-5} for NACA0012, NACA4412 and NACA4415. For the thin symmetric airfoil (NACA0012), the modified TE shapes show no benefit such as reducing drag, whilst the asymmetric NACA4412 show the 0.5% and 1.6% of drag reduction for saw-toothed and sine-curved TE shapes, respectively, compared with the standard TE. For a thicker asymmetric airfoil (NACA4415) with saw-toothed TE shape shows the drag increment of 2.4% compared with the standard TE. The NACA4415 with sine-curved TE shows the result of drag reduction up to 4.5% compare to standard TE.

The C_D results of NACA0012, NACA4412 and NACA4415 with different trailing edges at Re=1.05×10^5 shows in Figure 12. NACA4412's results show very small change of drag for different TE shape. Sine-curved TE shows the benefit of drag reduction for asymmetric airfoil.

5. Conclusion and Suggestion

The influence of saw-toothed and sine-curved trailing edge shape to the asymmetric aerofoils; NACA4412 and NACA4415 with three trailing edge shapes: standard straight line, saw-toothed and sine-curved shapes are numerical investigate at the chord Reynolds number 1.05×10^5. The CFD RANS-SST with a commercial code ANSYS CFX simulation is selected. The model is set up as fully submerged aerofoil with the chord length of 0.15 m and the span-width is 0.29 m. The fluid domain is modelled as working section area of 0.3×0.3 m and 3.30 m long. The NACA0012 study is performed so as to be used as the benchmark case for this study.

Firstly, the impact of the trailing edge shapes to the wake-flow behaviour is shown. Secondly, the drag coefficient is calculated and compared with the symmetric aerofoil NACA0012. The results show that the thicker camber, the higher drag coefficient for saw-toothed trailing edge shape. The sine-curved trailing edge provided drag results as the standard trailing edge for NACA0012 and NACA4412. The result suggests that, in term of drag consideration, it is interchangeable for using either NACA4412 or NACA4415 with sine-curved TE at this Re, as they are provided similar drag.

Finally, the results suggest the potential of using sine-curved TE shape for a thick asymmetric aerofoil in term of reducing the aerodynamic drag.

Acknowledgement

The authors acknowledge the associated support services at the University of Southampton, in the completion of this work.

References

[1] Oerlemans, S., Fisher, M., Maeder, T. and Kogler, K. (2009) Reduction of wind turbine noise using optimized airfoils and trailing-edge serrations. *AIAA journal*, 47, pp. 1470–1481.

[2] Gruber, M. (2012) Airfoil noise reduction by edge treatments. *University of Southampton, Faculty of Engineering and the Environment, Doctoral Thesis*, 229pp.

[3] Zhu, W. and Shen, W. (2015) Airfoil Trailing Edge Noise Generation and Its Surface Pressure Fluctuation. *Journal of Power and Energy Engineering*, **3**, 14-19. doi: 10.4236/jpee.2015.37003.

[4] Eleni, D.C ., Athanasios, T. I. and Dionissios, M. P. (2012) Evaluation of the turbulence models for the simulation of the flow over a National Advisory Committee for Aeronautics (NACA) 0012 airfoil. *Journal of Mechanical Engineering Research*, 4(3), pp. 100-111.
[5] Rattanasiri, P, Wilson P.A. and Phillips, A.B. (2014). Numerical Investigation of a fleet of towed AUVs. *Ocean Engineering*. vol 80C: pp. 25-35.
[6] Rattanasiri, P, Wilson P.A. and Phillips, A.B. (2013). Numerical Investigation of a pair of self-propelled AUVs operating in tandem. *Ocean Engineering.* vol. 100, pp 126-137.